Nigerian Journal of Theoretical and Environmental Physics (NJTEP)
ISSN Print: 3026-9601
DOI: https://doi.org/10.62292/njtep.v2i2.2024.34
Volume 2(2), June 2024

Analytical Analysis of the Bladeless Rotor Turbine Design for Enhanced Performance

[1]Olutayo Kehinde Onanuga, [2]Gbeminiyi Musibau Sobamowo, [3]Emmanuel Olusegun Ehinlafa, [4]Nald Erusiafe, [4]Muteeu Abayomi Olopade and [5]Matthew Iwada Ekum

[1]Department of Physical Sciences, College of Basic Sciences, Lagos State University of Science and Technology, Ikorodu, Nigeria
[2]Department of Mechanical Engineering, Faculty of Engineering, University of Lagos, Akoka, Lagos, Nigeria
[3]Department of Physics, Faculty of Science, University of Ilorin, Kwara State, Nigeria
[4]Department of Physics, Faculty of Science, University of Lagos, Akoka, Lagos, Nigeria
[5]Department of Mathematical Sciences, College of Basic Sciences, Lagos State University of Science and Technology, Ikorodu, Nigeria

*Corresponding author's email: onanuga.ko@lasustech.edu.ng
ORCID: https://orcid.org/0000-0001-9221-9971

ABSTRACT

The growing desire for clean and efficient energy solutions has fueled considerable advances in turbine technology. This study proposed a conceptual approach to enhancing the performance of bladeless turbines using an analytical technique, and the analytical solutions bear a resemblance to the experimental setup for a fluid dynamics investigation of a rotor for real-flow effects. The Navier-Stokes equations for fluid flow in cylindrical coordinates were simplified to two-dimensional flow by ignoring axial direction and velocity, and direct integration was used in conjunction with series expansion solutions. The experiment data were used to verify the rotor's fluid dynamics analytical solutions. The model's result was compared to previously calculated solutions of the fluid dynamics of a disc rotor in a bladeless turbine. The disc turbine models were used to predict radial velocity, tangential velocity, pressure gradient, volumetric flow rate, rotor torque, shear stress on the inner and outer disc walls, and rotor efficiency. The model was validated using experimental data with an efficiency of 23.9%, the theoretical solution model was 34%, and the analytical efficiency was 24.3%. The efficiency comparison of the analytical solutions model to the theoretical solutions model revealed a substantial difference, however, the correlation between computed theoretical and analytical results is significant. Previous studies used computed solutions for models, but current analytical solutions outperformed them. The model's output will be valuable to engineers building the disc turbine. It demonstrates a strong link between the analytical and experimental research of the bladeless turbine.

Keywords:
Bladeless rotor turbine,
Correlational analysis,
Energy efficiency,
Fluid Dynamics,
Renewable Energy.

INTRODUCTION

A turbine system is a mechanism that transmits energy between an incessant fluid flow and a blade scheme that spins constantly. The flow-generated forces govern the energy exchange. The flow's energy is initially employed to power a rotor, which is a rotating component. Nikola Tesla invented a friction centripetal turbine in 1913. The invention exploits the thin layer of flow rather than, as in a typical turbine, a fluid impinging on the blades. The bladeless turbine uses the working fluid's thin layer to transmit momentum between the fluid flow and the discs (Sengupta and Guha,2018). Consequently, it is dependent on forces of friction and viscosity, which reduce the efficiency of traditional turbines. Bladeless technology accomplishes energy in a useful and effective way, particularly in electric and hydraulic power generation (Hamdan et al., 2024).

The bladeless turbine is a rotating fluid device that operates with compressible and incompressible fluids. In literature, it is known as boundary-layered turbomachinery, corotating disc, and shear force. The existing energy generation capacity in developing countries is insufficient to meet the energy demands of

the citizenry (Wang,Zhu, Chen and Zhou, 2022). The increasing demand for electricity in developing countries is a source of concern; hence, it is vital to investigate other means of energy generation, one of which is the bladeless turbine (Onanuga, Erusiafe, Olopade and Chendo, 2020). The energy crisis is one of the most serious concerns confronting emerging countries, particularly Nigeria (Olujobi, Okorie, Olarinde and Aina-Pelemo, 2023).

There is inadequate electricity generation to meet the nation's standard requirements based on population growth (Emetele, Agubo and Chikwendu, 2021). Approximately 85 million Nigerians do not have access to grid electricity. Nigeria has the most significant energy deficit in the world with a population of 43.3% (Sani and Scholz, 2022).

Nigeria's power generation exploitation stands at 31%, which is less than the country's energy objective, implying an urgent need for power generation (Oyedepo, 2012). Rice, (1965) reported an experimental efficiency of 18.8% at 10000 rpm in an analytical and experimental study of corotating disc turbines. The spacing between the discs, fluid flow characteristics, velocity ratio, disc surface condition, radii ratio, and axial alignments between the rotor and the housing are recognized as critical variables influencing disc turbomachinery performance and efficiency (Caims, 2003). The Tesla turbine's reliability in turbulent flow was evaluated using a one-dimensional model (Song et al., 2018). They reported their turbine's theoretical flow analysis without reporting the disc turbine's analytical solutions.

An analytical and experimental study of a corotating disc turbine (Onanuga et al., 2020) used an air moisture regulator in the design and reported an experimental efficiency of 23.9% with a computed efficiency of 34% at 944.31 rad/s. Ciapp,Fiaschi,Niknam and Talluri, (2019) revealed that the flow within a Tesla turbine rotor was studied computationally without revealing the rotor's analytical solutions. One disadvantage of completing a fluid dynamics analysis of a rotor for compressible fluid utilized for low power in disc turbines is the anxiety involved in achieving optimal results. As a result, the study developed a rotor analytical model to provide better analytical solutions for improving the performance of the bladeless turbine's dynamics rotor, which was validated with experimental data and compared to the computed model (Onanuga et al, 2020 and Zhang et al, 2022).

The study presents an analytical analysis of bladeless rotor turbine design aimed at enhancing performance efficiency and reliability. The study validates its findings by using a mathematical model to predict the radial and tangential velocities, pressure gradients, Reynolds numbers, and Mach numbers of the working fluid through comparative analysis with experimental data and previous models. The study would be significant to energy companies, as they would benefit from bladeless turbines' efficiency and reduced costs, enhancing profitability and reliability. Government agencies can promote sustainable energy, meeting efficiency goals and cutting emissions. Environmental groups see reduced impacts, supporting conservation. Universities advance research, and businesses save costs. Remote communities gain reliable power, and investors find profitable opportunities.

Theoretical Consideration and Problem formulation

The continuity and Navier-Stokes equations in a cylinder (r, θ, z) were used for a theoretical fluid flow analysis in the turbine rotor. The entry flow is uniform at the rotor outside edge. The flow field is the same at any angle θ due to the uniformity at the outer edge of the rotor. The flow field is believed to be radially symmetrical, $\frac{\partial P}{\partial \theta}$ is insignificant in comparison to the wall friction forces. The theoretical flow model analysis in radial and tangential velocity distributions between co-rotating, and parallel discs is illustrated in Figure 1.

Figure 1: Rotor flow decomposed into cylindrical coordinates

The axial body force is insignificant, and a two-dimensional assumption of fluid flow in radial and tangential velocity distributions between co-rotating parallel discs is developed.

Conservation of Mass (Antoine Lavoisier):

$$\frac{\partial u}{\partial r}+\frac{u}{r}=0, \quad (1)$$

Conservation of Momentum (Navier-Stokes Equation):

r-direction momentum

$$u\frac{\partial u}{\partial r}-\frac{v^2}{r}=f_r-\frac{1}{\rho}\frac{\partial p}{\partial r}+\nu\left[\frac{\partial^2 u}{\partial r^2}+\frac{1}{r}\frac{\partial u}{\partial r}+\frac{\partial^2 u}{\partial z^2}-\frac{u}{r^2}\right], \quad (2)$$

θ-direction momentum

$$u\frac{\partial v}{\partial r}+\frac{uv}{r}=f_\theta+\nu\left[\frac{\partial^2 v}{\partial r^2}+\frac{1}{r}\frac{\partial v}{\partial r}+\frac{\partial^2 v}{\partial z^2}-\frac{v}{r^2}\right], \quad (3)$$

z-direction momentum

$$0=-\frac{1}{\rho}\frac{\partial p}{\partial z}, \quad (4)$$

Equation (4) reveals that at any (r, θ) position, there is uniform pressure across the flow channel. The appropriate boundary conditions for the flow process are given in equation 5.

$$\begin{aligned} &r=r_i, 0\le z\le b, u=u_i, \quad v=v_i\ w=0\\ &r=r_o, 0\le z\le b, p=0, \quad u=u_0, \quad v=v_0,\ w=0\\ &z=0, r_i\le r\le r_0, \quad u=0, \quad v=\omega r, w=0\\ &z=b, r_i\le r\le r_0, \quad u=0, \quad v=\omega r, w=0 \end{aligned} \quad (5)$$

According to Song et al, (2018), the viscous drag imposed on the flow by the disc side walls is addressed and modelled as the body force acting on the flow in each direction. Equations (2) and (3) are written as

r-direction momentum

$$u\frac{\partial u}{\partial r}-\frac{v^2}{r}=-\frac{1}{\rho}\frac{\partial p}{\partial r}+f_r, \quad (6)$$

θ-direction momentum

$$u\frac{\partial v}{\partial r}+\frac{uv}{r}=f_\theta, \quad (7)$$

The following f_r, f_θ represents the body force influencing the flow in each direction:

$$f_r=\frac{12\mu}{\rho b^2}u \quad (8)$$

$$f_\theta=-\frac{12\mu}{\rho b^2}(v-\omega r) \quad (9)$$

Also, recall that Equation (1), is represented as

$$\frac{\partial u}{\partial r}=-\frac{u}{r}, \quad (10)$$

Substitute Equations. (8) and (10) into Equation. (6), we have

$$-\frac{u^2}{r}-\frac{v^2}{r}=-\frac{1}{\rho}\frac{\partial p}{\partial r}+\frac{12\mu}{\rho b^2}u, \quad (11)$$

We can write Equation 11 as

$$\frac{\partial p}{\partial r}=\frac{12}{b^2}u+\frac{\rho u^2}{r}+\frac{\rho v^2}{r}, \quad (12)$$

Recall that $u=-\frac{\dot{m}_c}{2\pi r b\rho}$

Substitute $u=-\frac{\dot{m}_c}{2\pi r b\rho}$ into Equation 11 to become Equation 13

$$\frac{\partial p}{\partial r}=-\frac{12\mu}{b^2}\left(\frac{\dot{m}_c}{2\pi r b}\right)+\frac{\rho}{r}\left(\frac{\dot{m}_c}{2\pi r b\rho}\right)^2+\frac{\rho v^2}{r}, \quad (13)$$

Substitute $u=-\frac{\dot{m}_c}{2\pi r b}$ and Equation 9 into Equation 7, we have,

$$-\frac{\dot{m}_c}{2\pi r}\frac{\partial v}{\partial r}-\frac{\dot{m}_c}{2\pi r b\rho}\frac{v}{r}=-\frac{12\mu}{\rho b^2}(v-\omega r), \quad (14)$$

We can express Equation (14) as

$$\frac{\partial v}{\partial r}+\left(\frac{1}{r}-\frac{24\mu\pi r}{\dot{m}_c b}\right)v=-\frac{24\mu\pi\omega^{\ 2}}{\dot{m}_c b}, \quad (15)$$

Equation (15) is represented as

$$\frac{\partial v}{\partial r}+\left(\frac{1}{r}-\beta r\right)v=-\beta\omega r^2, \quad (16)$$

Where $\beta=\frac{24\mu\pi}{\dot{m}_c b}$

Method of Solution: Analytical solutions of the theoretical flow models of the turbine

The initial condition as

$$r=r_i, v=v_o \quad (17)$$

Using the Integrating factor approach for Equation (16), we have

$$\frac{d}{dr}\left[re^{-\frac{\beta r^2}{2}}v\right]=-\beta\omega r^2\left[re^{-\frac{\beta r^2}{2}}\right], \quad (18)$$

Integrating both sides of Equation (18), we have

$$re^{-\frac{\beta r^2}{2}}v=-\beta\omega\int r^3 e^{-\frac{\beta r^2}{2}}dr, \quad (19)$$

The term at the RHS of Equation (19) could not be integrated directly. To generate an analytical model for the equation, we adopted Taylor's series expansion for the exponential term as

$$e^{-\frac{\beta r^2}{2}}=e^{-\frac{\beta r_i^2}{2}}\left[1-\beta r_i(r-r_i)+\frac{(r-r_i)^2}{2!}[\beta^2 r_i^2-\beta]+\frac{(r-r_i)^3}{3!}[3\beta^2 r_i-\beta^3 r_i^3]+\ldots\right]$$

$$r^3e^{-\frac{\beta r^2}{2}}=e^{-\frac{\beta r_i^2}{2}}\begin{bmatrix} r^3-\beta r_i(r^4-r_i r^3)+\frac{(r^5-2r_i r^4+r_i^2 r^3)}{2!}[\beta^2 r_i^2-\beta] \\ +\frac{(r^6-3r_i r^5+3r_i^2 r^4-r_i^3 r^3)}{3!}[3\beta^2 r_i-\beta^3 r_i^3]+\ldots \end{bmatrix} \quad (20)$$

Integration of Equation (20) is given as

$$\int r^3 e^{-\frac{\beta r^2}{2}}dr=e^{-\frac{\beta r_i^2}{2}}\begin{bmatrix} \frac{r^4}{4}-\beta r_i\left(\frac{r^5}{5}-r_i\frac{r^4}{4}\right)+\frac{\beta(\beta r_i^2-1)}{2!}\left(\frac{r^6}{6}-\frac{2r_i r^5}{5}+\frac{r_i^2 r^4}{4}\right) \\ -\frac{\beta^2 r_i(\beta r_i^2-3)}{3!}\left(\frac{r^7}{7}-\frac{r_i r^6}{2}+\frac{3r_i^2 r^5}{5}-\frac{r_i^3 r^4}{4}\right)+\ldots \end{bmatrix}+c, \quad (21)$$

Integrating Equation (18) and v the subject of the equation as in Equation (22)

$$v = v_i + \frac{\beta}{r_i}\omega r_i^4\left[\frac{1}{4} + \frac{\beta r_i^2}{20} + \frac{\beta r_i^2(\beta r_i^2-1)}{120} - \frac{\beta^2 r_i^4(\beta r_i^2-3)}{840} + \ldots\right]$$
$$-\frac{\beta}{r}\omega e^{-\frac{\beta\left(r_i^2-r^2\right)}{2}}\begin{bmatrix}\frac{r^4}{4} - \beta r_i\left(\frac{r^5}{5} - r_i\frac{r^4}{4}\right) + \frac{\beta(\beta r_i^2-1)}{2!}\left(\frac{r^6}{6} - \frac{2r_i r^5}{5} + \frac{r_i^2 r^4}{4}\right)\\ -\frac{\beta^2 r_i(\beta r_i^2-3)}{3!}\left(\frac{r^7}{7} - \frac{r_i r^6}{2} + \frac{3r_i^2 r^5}{5} - \frac{r_i^3 r^4}{4}\right) + \ldots\end{bmatrix}, \quad (22)$$

Equation (22) is substituted in Equation (13) to give

$$\frac{\partial p}{\partial r} = -\frac{12\mu}{b^2}\left(\frac{\dot{m}_c}{2\pi r b\rho}\right) + \frac{\rho}{r}\left(\frac{\dot{m}_c}{2\pi r b}\right)^2$$
$$+\frac{\rho}{r}\left\{\begin{matrix}v_i + \frac{\beta}{r_i}\omega r_i^4\left[\frac{1}{4} + \frac{\beta r_i^2}{20} + \frac{\beta r_i^2(\beta r_i^2-1)}{120} - \frac{\beta^2 r_i^4(\beta r_i^2-3)}{840} + \ldots\right]\\ -\frac{\beta}{r}\omega e^{-\frac{\beta\left(r_i^2-r^2\right)}{2}}\begin{bmatrix}\frac{r^4}{4} - \beta r_i\left(\frac{r^5}{5} - r_i\frac{r^4}{4}\right) + \frac{\beta(\beta r_i^2-1)}{2!}\left(\frac{r^6}{6} - \frac{2r_i r^5}{5} + \frac{r_i^2 r^4}{4}\right)\\ -\frac{\beta^2 r_i(\beta r_i^2-3)}{3!}\left(\frac{r^7}{7} - \frac{r_i r^6}{2} + \frac{3r_i^2 r^5}{5} - \frac{r_i^3 r^4}{4}\right) + \ldots\end{bmatrix}\end{matrix}\right\}^2, \quad (23)$$

The volumetric flow rate is obtained as

$$Q = \int_0^{2\pi}\int_{r_i}^{r_o} v r dr d\theta \quad (24)$$

Equation (24) is written as

$$Q = \int_0^{2\pi}\int_{r_i}^{r_o}\left\{\begin{matrix}v_i r + \beta\omega r_i^3 r\left[\frac{1}{4} + \frac{\beta r_i^2}{20} + \frac{\beta r_i^2(\beta r_i^2-1)}{120} - \frac{\beta^2 r_i^4(\beta r_i^2-3)}{840} + \ldots\right]\\ -\beta\omega\begin{bmatrix}1 + \beta r_i(r-r_i) + \beta\frac{(r-r_i)^2}{2!}[\beta r_i^2+1]\\ +\beta^2 r_i\frac{(r-r_i)^3}{3!}[\beta r_i^2+3] + \ldots\end{bmatrix}\begin{bmatrix}\frac{r^4}{4} - \beta r_i\left(\frac{r^5}{5} - \frac{r_i r^4}{4}\right) + \frac{\beta(\beta r_i^2-1)}{2!}\left(\frac{r^6}{6} - \frac{2r_i r^5}{5} + \frac{r_i^2 r^4}{4}\right)\\ -\frac{\beta^2 r_i(\beta r_i^2-3)}{3!}\left(\frac{r^7}{7} - \frac{r_i r^6}{2} + \frac{3r_i^2 r^5}{5} - \frac{r_i^3 r^4}{4}\right) + \ldots\end{bmatrix}\end{matrix}\right\} dr d\theta \quad (25)$$

Integrate Equation (25) with respect to θ, we have

$$Q = \pi\omega r_i(r_o^2 - r_i^2) + \beta\pi\omega r_i^3(r_o^2 - r_i^2)\left[\frac{1}{4} + \frac{\beta r_i^2}{20} + \frac{\beta r_i^2(\beta r_i^2-1)}{120} - \frac{\beta^2 r_i^4(\beta r_i^2-3)}{840} + \ldots\right]$$
$$-2\pi\beta\omega\left\{\begin{matrix}\begin{bmatrix}\frac{r^5}{20} - \beta r_i\left(\frac{r^6}{30} - \frac{r_i r^5}{20}\right) + \frac{\beta(\beta r_i^2-1)}{2!}\left(\frac{r^7}{42} - \frac{2r_i r^6}{30} + \frac{r_i^2 r^5}{20}\right)\\ -\frac{\beta^2 r_i(\beta r_i^2-3)}{3!}\left(\frac{r^8}{56} - \frac{r_i r^7}{14} + \frac{3r_i^2 r^6}{30} - \frac{r_i^3 r^5}{20}\right) + \ldots\end{bmatrix}\\ +\beta r_i\begin{bmatrix}\frac{r^6}{24} - \beta r_i\left(\frac{r^7}{35} - \frac{r_i r^6}{24}\right) + \frac{\beta(\beta r_i^2-1)}{2!}\left(\frac{r^8}{48} - \frac{2r_i r^7}{35} + \frac{r_i^2 r^6}{24}\right)\\ -\frac{\beta^2 r_i(\beta r_i^2-3)}{3!}\left(\frac{r^9}{63} - \frac{r_i r^8}{16} + \frac{3r_i^2 r^7}{35} - \frac{r_i^3 r^6}{24}\right) + \ldots\end{bmatrix}\\ -\beta r_i^2\begin{bmatrix}\frac{r^5}{20} - \beta r_i\left(\frac{r^6}{30} - \frac{r_i r^5}{20}\right) + \frac{\beta(\beta r_i^2-1)}{2!}\left(\frac{r^7}{42} - \frac{2r_i r^6}{30} + \frac{r_i^2 r^5}{20}\right)\\ -\frac{\beta^2 r_i(\beta r_i^2-3)}{3!}\left(\frac{r^8}{56} - \frac{r_i r^7}{14} + \frac{3r_i^2 r^6}{30} + \frac{r_i^3 r^5}{20}\right) + \ldots\end{bmatrix} + \ldots\end{matrix}\right\} \quad (26)$$

The shear forces on the disc's interior and exterior walls are

$$\tau_i = \mu\frac{dv}{dr}\Big|_{r_i}, \qquad \tau_o = -\mu\frac{dv}{dr}\Big|_{r_o}$$

From Equation (18), we have

$$\frac{dv}{dr} = -\beta\omega\left\{\begin{matrix}e^{-\frac{\beta\left(r_i^2-r^2\right)}{2}}\begin{bmatrix}\frac{3r^2}{4} - \beta r_i\left(\frac{4r^3}{5} - \frac{3r^2 r_i}{4}\right) + \frac{\beta(\beta r_i^2-1)}{2!}\left(\frac{5r^4}{6} - \frac{8r_i r^3}{5} + \frac{3r_i^2 r^2}{4}\right)\\ -\frac{\beta^2 r_i(\beta r_i^2-3)}{3!}\left(\frac{6r^5}{7} - \frac{5r_i r^4}{2} + \frac{12r_i^2 r^3}{5} - \frac{3r_i^3 r^2}{4}\right) + \ldots\end{bmatrix}\\ +\beta r e^{-\frac{\beta\left(r_i^2-r^2\right)}{2}}\begin{bmatrix}\frac{r^3}{4} - \beta r_i\left(\frac{r^4}{5} - \frac{r^3 r_i}{4}\right) + \frac{\beta(\beta r_i^2-1)}{2!}\left(\frac{r^5}{6} - \frac{2r_i r^4}{5} + \frac{r_i^2 r^3}{4}\right)\\ -\frac{\beta^2 r_i(\beta r_i^2-3)}{3!}\left(\frac{r^6}{7} - \frac{r_i r^5}{2} + \frac{3r_i^2 r^4}{5} - \frac{r_i^3 r^3}{4}\right) + \ldots\end{bmatrix}\end{matrix}\right\}, \quad (27)$$

Therefore, the shear force on the inner wall of the disc is simply to

$$\tau_i = -\mu\beta\omega r_i^2\left\{\begin{matrix}\left[\frac{3}{4} - \frac{\beta r_i^2}{20} - \frac{\beta r_i^2(\beta r_i^2-1)}{120} - \frac{\beta^2 r_i^4(\beta r_i^2-3)}{840} + \ldots\right]\\ +\beta r_i^2\left[\frac{1}{4} + \frac{\beta r_i^2}{20} + \frac{\beta r_i^2(\beta r_i^2-1)}{120} + \frac{\beta^2 r_i^4(\beta r_i^2-3)}{840} + \ldots\right]\end{matrix}\right\} \quad (28)$$

In addition, the shear force on the outer wall of the disc is

$$\tau_o = \mu\beta\omega e^{-\frac{\beta\left(r_i^2-r_o^2\right)}{2}}\left\{\begin{matrix}\left[\begin{matrix}\frac{3r_o^2}{4}-\beta r_i\left(\frac{4r_o^3}{5}-\frac{3r_o^2r_i}{4}\right)+\frac{\beta(\beta r_i^2-1)}{2!}\left(\frac{5r_o^4}{6}-\frac{8r_ir_o^3}{5}+\frac{3r_i^2r_o^2}{4}\right)\\ -\frac{\beta^2r_i(\beta r_i^2-3)}{3!}\left(\frac{6r_o^5}{7}-\frac{5r_ir_o^4}{2}+\frac{12r_i^2r_o^3}{5}+\frac{3r_i^3r_o^2}{4}\right)+\ldots\end{matrix}\right]\\ +\beta r_o\left[\begin{matrix}\frac{r_o^3}{4}-\beta r_i\left(\frac{r_o^4}{5}-\frac{r_o^3r_i}{4}\right)+\frac{\beta(\beta r_i^2-1)}{2!}\left(\frac{r_o^5}{6}-\frac{2r_ir_o^4}{5}+\frac{r_i^2r_o^3}{4}\right)\\ -\frac{\beta^2r_i(\beta r_i^2-3)}{3!}\left(\frac{r_o^6}{7}-\frac{r_ir_o^5}{2}+\frac{3r_i^2r_o^4}{5}+\frac{r_i^3r_o^3}{4}\right)+\ldots\end{matrix}\right]\end{matrix}\right\} \quad (29)$$

Following (Rusin et al, 2018), the rotor power output is given as

$$P_{rotor} = \int_{r_i}^{r_o}\frac{6\mu}{b}(2\pi r)rdr = \frac{12\pi\mu}{b}\int_{r_i}^{r_o} vr^2dr \quad (30)$$

Again, recall from Equation (22) that

$$v = v_i + \frac{\beta}{r_i}\omega r_i^4\left[\frac{1}{4}+\frac{\beta r_i^2}{20}+\frac{\beta r_i^2(\beta r_i^2-1)}{120}-\frac{\beta^2r_i^4(\beta r_i^2-3)}{840}+\ldots\right]$$

$$-\frac{\beta}{r}\omega e^{-\frac{\beta(r_i^2-r^2)}{2}}\left[\begin{matrix}\frac{r^4}{4}-\beta r_i\left(\frac{r^5}{5}-r_i\frac{r^4}{4}\right)+\frac{\beta(\beta r_i^2-1)}{2!}\left(\frac{r^6}{6}-\frac{2r_ir^5}{5}+\frac{r_i^2r^4}{4}\right)\\ -\frac{\beta^2r_i(\beta r_i^2-3)}{3!}\left(\frac{r^7}{7}-\frac{r_ir^6}{2}+\frac{3r_i^2r^5}{5}-\frac{r_i^3r^4}{4}\right)+\ldots\end{matrix}\right],$$

Therefore,

$$P_{output} = \frac{12\pi\mu}{b}\left[\begin{matrix}\frac{v_i(r_o^3-r_i^3)}{3}+\frac{\beta}{r_i}\omega r_i^4(r_o^3-r_i^3)\left[\frac{1}{12}+\frac{\beta r_i^2}{60}+\frac{\beta r_i^2(\beta r_i^2-1)}{360}-\frac{\beta^2r_i^4(\beta r_i^2-3)}{2520}+\ldots\right]\\ -\beta\omega(r_o^6-r_i^6)\left[\begin{matrix}\frac{(r_o^6-r_i^6)}{24}-\beta r_i\left(\frac{(r_o^7-r_i^7)}{35}-\frac{r_i(r_o^6-r_i^6)}{24}\right)+\frac{\beta(\beta r_i^2-1)}{2!}\left(\frac{(r_o^8-r_i^8)}{48}-\frac{2r_i(r_o^7-r_i^7)}{35}+\frac{r_i^2(r_o^6-r_i^6)}{24}\right)\\ -\frac{\beta^2r_i(\beta r_i^2-3)}{3!}\left(\frac{(r_o^9-r_i^9)}{63}-\frac{r_i(r_o^8-r_i^8)}{16}+\frac{3r_i^2(r_o^7-r_i^7)}{35}-\frac{r_i^3(r_o^6-r_i^6)}{24}\right)+\ldots\end{matrix}\right]\end{matrix}\right] \quad (31)$$

The torque of the rotor as$T = \frac{P_{output}}{\omega}$, which gives

$$T = \frac{12\pi\mu}{\omega b}\left[\begin{matrix}\frac{v_i(r_o^3-r_i^3)}{3}+\frac{\beta}{r_i}\omega r_i^4(r_o^3-r_i^3)\left[\frac{1}{12}+\frac{\beta r_i^2}{60}+\frac{\beta r_i^2(\beta r_i^2-1)}{360}-\frac{\beta^2r_i^4(\beta r_i^2-3)}{2520}+\ldots\right]\\ -\beta\omega(r_o^6-r_i^6)\left[\begin{matrix}\frac{(r_o^6-r_i^6)}{24}-\beta r_i\left(\frac{(r_o^7-r_i^7)}{35}-\frac{r_i(r_o^6-r_i^6)}{24}\right)+\frac{\beta(\beta r_i^2-1)}{2!}\left(\frac{(r_o^8-r_i^8)}{48}-\frac{2r_i(r_o^7-r_i^7)}{35}+\frac{r_i^2(r_o^6-r_i^6)}{24}\right)\\ -\frac{\beta^2r_i(\beta r_i^2-3)}{3!}\left(\frac{(r_o^9-r_i^9)}{63}-\frac{r_i(r_o^8-r_i^8)}{16}+\frac{3r_i^2(r_o^7-r_i^7)}{35}-\frac{r_i^3(r_o^6-r_i^6)}{24}\right)+\ldots\end{matrix}\right]\end{matrix}\right] \quad (32)$$

According to (Krzysztof et al, 2019), the theoretical efficiency of the turbine is given as

$$\eta = \frac{P_{output}}{\dot{m}_cT_{in}c_p\left(1-\left(\frac{p_{out}}{p_{in}}\right)^{\frac{k-1}{k}}\right)} \quad (33)$$

Therefore, if the Equation. (31) is substituted into Equation (33), we have the theoretical efficiency of the turbine as

$$\eta = \frac{12\pi\mu}{b\dot{m}_cT_{in}c_p\left(1-\left(\frac{p_{out}}{p_{in}}\right)^{\frac{k-1}{k}}\right)}\left[\begin{matrix}\frac{v_i(r_o^3-r_i^3)}{3}+\frac{\beta}{r_i}\omega r_i^4(r_o^3-r_i^3)\left[\frac{1}{12}+\frac{\beta r_i^2}{60}+\frac{\beta r_i^2(\beta r_i^2-1)}{360}-\frac{\beta^2r_i^4(\beta r_i^2-3)}{2520}+\ldots\right]\\ -\beta\omega(r_o^6-r_i^6)\left[\begin{matrix}\frac{(r_o^6-r_i^6)}{24}-\beta r_i\left(\frac{(r_o^7-r_i^7)}{35}-\frac{r_i(r_o^6-r_i^6)}{24}\right)+\frac{\beta(\beta r_i^2-1)}{2!}\left(\frac{(r_o^8-r_i^8)}{48}-\frac{2r_i(r_o^7-r_i^7)}{35}+\frac{r_i^2(r_o^6-r_i^6)}{24}\right)\\ -\frac{\beta^2r_i(\beta r_i^2-3)}{3!}\left(\frac{(r_o^9-r_i^9)}{63}-\frac{r_i(r_o^8-r_i^8)}{16}+\frac{3r_i^2(r_o^7-r_i^7)}{35}-\frac{r_i^3(r_o^6-r_i^6)}{24}\right)+\ldots\end{matrix}\right]\end{matrix}\right] \quad (34)$$

Nomenclature

u	Fluid radial velocity (m/s)	$\dot{m}$	Mass flow rate (kg/s)
u_i	Inlet radial velocity (m/s)	z	axial direction
u_o	Outlet radial velocity (m/s)	r_i	Inner radius of the disc(m)
v	Fluid tangential velocity (m/s)	r_o	Outer radius of the disc(m)
w	Axial velocity (m/s)	ρ	Density of fluid(kg/m^3)
μ	Dynamic viscosity	Pi	Inlet pressure of turbine (N/m^2)
f_θ	The body force in tangential direction	Po	Outlet pressure of turbine (N/m2)
f_r	The body force in radial direction	b	Distance between two discs (mm)
ω	Angular velocity of discs (rad/s)	T	Torque
τ	Shear force		

RESULTS AND DISCUSSION

Results

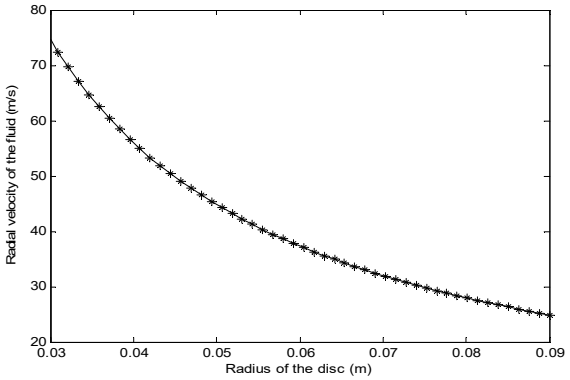

Figure 2: The expected radial velocity of the working fluid varies with the disc radius.

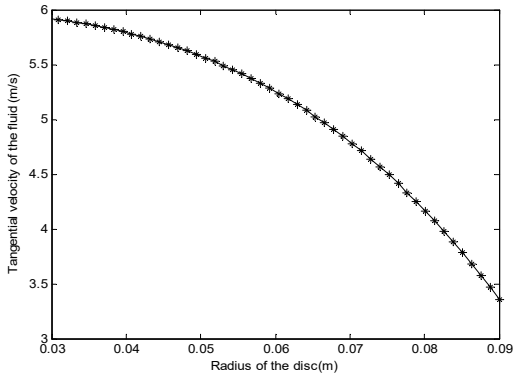

Figure 3: The tangential velocity of the working fluid depends on the disc radius

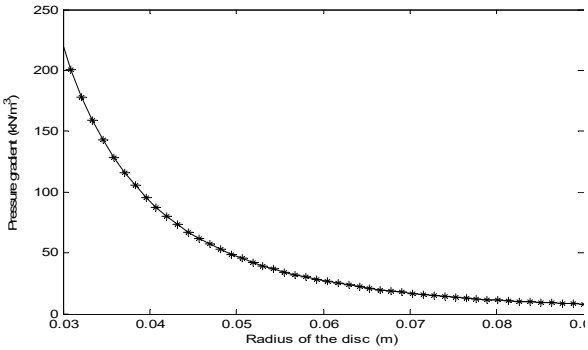

Figure 4: The working fluid pressure gradient varies with the disc radius.

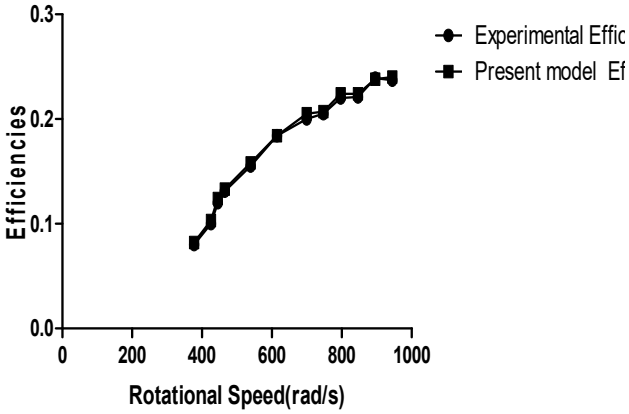

Figure 5: Efficiency comparisons between experimental and current models.

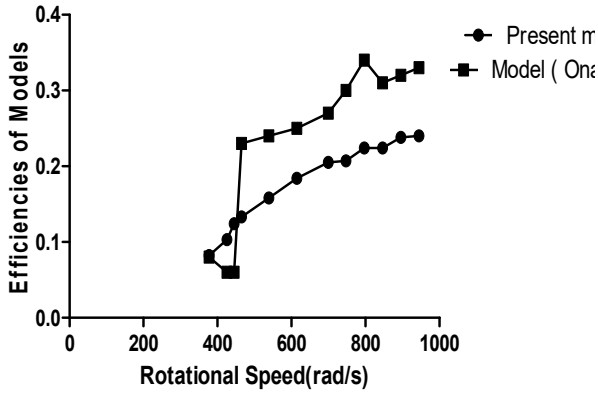

Figure 6: Comparison of turbine Reynolds number experimental and model outcomes

Figure 7: Comparison of the turbine Mach number experimental and model outcomes.

Figures 2-7 show the result of the predictions. Figure 2 depicts the expected radial velocity of the working fluid at the disc radius. The radial velocity increases with increasing radius, suggesting the fluid moves outward. Figure 3 illustrates the tangential velocity variation of the working fluid with disc radius. The tangential velocity increases with the radius, which is expected due to the conservation of angular momentum in a rotating system. Figure 4 displays the pressure gradient variation with disc radius. The pressure gradient decreases as the radius increases, suggesting a reduction in pressure as the fluid moves outward. Figure 5 compares the experimental and present model efficiencies. The model shows higher efficiency than the experimental results, validating the model's effectiveness in predicting turbine performance. Figure 6 compares the turbine Reynolds number between experimental and model outcomes. Both show similar trends, indicating the model's accuracy in predicting flow characteristics. Figure 7 compares the turbine Mach number between experimental and model outcomes. The results align closely, further confirming the model's reliability.

Table 1: Comparison of Present model efficiency to Experimental result (Onanuga et al., 2020) Two-way Anova (Bonferroni posttest)

Rotational Speed(rad/s)	Efficiency Experiment	Efficiency model	Difference	95% Cl of difference	t-Test	P value	Summary
380	0.080	0.082	0.002	-0.004 to 0.008	1.2	P > 0.05	NS
430	0.100	0.103	0.003	-0.003 to 0.009	1.8	P > 0.05	NS
440	0.120	0.124	0.004	-0.002 to 0.010	2.4	P > 0.05	NS
460	0.131	0.133	0.002	-0.004 to 0.008	1.2	P > 0.05	NS
540	0.155	0.158	0.003	-0.003 to 0.009	1.8	P > 0.05	NS
610	0.184	0.184	0.000	-0.006 to 0.006	0.0	P > 0.05	NS
700	0.200	0.205	0.005	-0.001 to 0.011	3.0	P > 0.05	NS
750	0.205	0.207	0.002	-0.004 to 0.008	1.2	P > 0.05	NS
800	0.220	0.224	0.004	-0.002 to 0.010	2.4	P > 0.05	NS
850	0.221	0.224	0.003	-0.003 to 0.009	1.8	P > 0.05	NS
900	0.239	0.238	-0.001	-0.007 to 0.005	0.6	P > 0.05	NS
940	0.237	0.240	0.003	-0.003 to 0.009	1.8	P > 0.05	NS

Table 2: Comparison of Present model efficiency to Model efficiency (Onanuga et al., 2020) Two-way Anova (Bonferroni posttest)

Rotational Speed(rad/s)	Present mo efficiency	model efficie (Onanuga et 2020)	Difference	95% Cl difference	t-Test	P value	Summary
380	0.082	0.080	-0.002	-0.21 to 0.21	0.0	P > 0.05	NS
430	0.103	0.060	-0.043	-0.25 to 0.17	0.7	P > 0.05	NS
440	0.124	0.060	-0.064	-0.28 to 0.15	1.1	P > 0.05	NS
460	0.133	0.230	0.097	-0.11 to 0.31	1.7	P > 0.05	NS
540	0.158	0.240	0.082	-0.13 to 0.29	1.4	P > 0.05	NS
610	0.184	0.250	0.066	-0.15 to 0.28	1.1	P > 0.05	NS
700	0.205	0.270	0.065	-0.15 to 0.28	1.1	P > 0.05	NS
750	0.207	0.300	0.093	-0.12 to 0.30	1.6	P > 0.05	NS
800	0.224	0.340	0.116	-0.10 to 0.33	2.0	P > 0.05	NS
850	0.224	0.310	0.086	-0.13 to 0.30	1.5	P > 0.05	NS
900	0.238	0.320	0.082	-0.13 to 0.29	1.4	P > 0.05	NS
940	0.240	0.330	0.090	-0.12 to 0.30	1.5	P > 0.05	NS

Table 3: Numeric comparison of the present model Reynold's and Mach numbers to Reynold's and Mach numbers (*Onanuga et al,2020*) results

Rotational Speed (ω) rad/s	Reynold's number (experimental result) *Onanuga et. al, 2020*	Reynold's number (present model result)	Mach number (experimental result) *Onanuga et al,2020*	Mach number (present model result)
377.040	211.030	205.780	0.017	0.018
425.220	238.000	232.410	0.020	0.020
444.800	248.960	243.330	0.020	0.021
464.490	259.980	254.630	0.021	0.022
538.850	269.000	263.580	0.022	0.023
614.160	343.750	338.690	0.028	0.029
699.100	391.290	385.330	0.032	0.033
747.200	418.210	412.240	0.034	0.035
796.460	445.780	440.460	0.037	0.037
845.750	473.370	468.690	0.039	0.040
895.030	500.950	495.210	0.042	0.043
944.310	528.530	523.080	0.044	0.045

Table 4: Covariance Analysis of Present model efficiency and Prototype efficiency (Onanuga et al., 2020).

Source of variation	Degree of freedom	Sum of Square(SS)	Mean Square (MS)	F- ratio	P-value	% of total variation
Present Model efficiency and Prototype efficiency	1.0	0.000038	0.000038	26.61	0.0003	0.06
Rotational Speed	11.0	0.067	0.0061	4330.65	0.0001	99.92
Residual (Error)	11.0	0.000015	0.0000014			
Total	23.0	0.067				

Table 5: Covariance Analysis of Present model efficiency and Model efficiency (Onanuga et al., 2020).

Source of variation	Degree of freedom	Sum of Square(SS)	Mean Square (MS)	F- ratio	P-value	% of total variation
Present model efficiency and Model efficiency	1.0	0.019	0.019	10.8	0.0003	10.57
Rotational Speed	11.0	0.14	0.013	7.3	0.0001	78.68
Residual (Error)	11.0	0.019	0.0017			
Total	23.0	0.18				

Table 1 compares the present model efficiency to the experimental results using a two-way ANOVA with Bonferroni posttest. The differences are minor and statistically insignificant ($P > 0.05$), indicating that the model aligns well with experimental data. Table 2 compares the present model efficiency to Onanuga et al. (2020) model efficiency. Although there are some differences, these are not statistically significant ($P > 0.05$), suggesting that both models predict similar efficiencies. Table 3 is the numeric comparison of Reynolds and Mach numbers between the present model and Onanuga et al, (2020) results. The values are close, indicating consistency and reliability in the model's predictions. Table 4 is the covariance analysis of present model efficiency and prototype efficiency. The rotational speed accounts for 99.92% of the variation, indicating its dominant effect on efficiency. Table 5 is a covariance analysis of present model efficiency and model efficiency (Onanuga et al, 2020). The rotational speed significantly affects efficiency, with 89.43% of the variation attributed to it.

Discussion

Figures 2-4 depict variations in the working fluid's radial velocity (u), and tangential velocity (v) for a varying radius and pressure gradient. As the working fluid passes through the rotor, as shown in Figure 2, its velocity decreases. The magnitude of radial velocity must increase to satisfy the equation of continuity as the working fluid passes from the rotor intake to the output.

Figure 3 demonstrates that as the working fluid moves slightly within the rotor, its tangential velocity decreases dramatically. The substantial velocity difference between the working fluid and the revolving disc results in significant wall friction. This implies that the working fluid's tangential velocity decreases as the friction force causes the discs to spin.

Figure 4 shows the pressure gradient as an indicator of rotor radius. The one-dimensional model accounts for the radial pressure gradient in the rotor. The working fluid flows into the disc, generating a pressure decrease that is interpreted as the force pushing the airflow out the rotor's outlet.

The analytical (model) and experimental efficiencies account for 0.01% of the total variation and have a P-value of 0.8455. As indicated in the Table 4, the P value of the experimental to model efficiencies is insignificant, with a minimal divergence between the model and experimental efficiency. This suggests that the experiment and the model have almost the same effect at all angular speed levels, as shown in Table 4, and the experimental efficiency confirmed the model's efficiency with an insignificant difference.

Tables 1, 2, and 3 show a numerical comparison of the outcomes of the experimental (Onanuga et al 2020) and empirical models of turbine efficiency, Reynold's, and Mach numbers in this work. Figures 5, 6, and 7 show graphical representations of the comparisons as well as the empirical model results. This is highly consistent with the findings of the experimental output. This shows that the empirical model is a reasonable choice for comparing the qualitative effects of various operating circumstances.

The study's policy implications include the finding that bladeless turbines outperform traditional designs. Policies should encourage their use in new and existing power plants to increase energy efficiency. Bladeless turbines, which are highly efficient and reliable, should be preferred in renewable energy projects. Governments and the commercial sector should collaborate to fund research and development. To solve Nigeria's shortage of electricity access, incorporating bladeless turbines into the national grid can help.

Policies should focus on infrastructure development in remote and underserved areas. Bladeless turbines align with SDGs, including affordable and clean energy (Goal 7) and industry, innovation, and infrastructure (Goal 9). Policymakers should integrate these technologies into national strategies. Educational institutions should develop specialized programs to train engineers and technicians in bladeless turbine technology. Policies should encourage partnerships between universities and industry for knowledge transfer. Bladeless turbines reduce mechanical wear and maintenance, offering a cleaner alternative. Environmental policies should support technologies that minimize ecological footprints for sustainability.

CONCLUSION

The work has developed an analytical solution for the dynamics rotor of turbines and experimental data were used to validate the developed analytical solutions. The model's Tesla turbine efficiency projection is consistent with the experimental results. The simulations also showed that the working fluid's radial velocity drops as it moves through the rotor. The tangential velocity drops dramatically when the working fluid moves somewhat inward within the rotor, indicating high wall friction due to the significant speed differential between the working fluid and the revolving disc. The tangential velocity of the working fluid drops when the discs are forced to rotate due to friction. The developed model provided useful information on fluid flow characteristics that would aid in the design and construction of the bladeless turbine.

The study recommends that policymakers and energy sector stakeholders should prioritize the adoption of bladeless turbine technology in new and existing power generation projects. The higher efficiency and lower maintenance requirements make these turbines a valuable addition to energy infrastructures. Governments, academic institutions, and private sector entities should increase funding for research and development in bladeless turbine technology. This investment should focus on optimizing design parameters, improving materials, and enhancing computational models to further increase efficiency and reliability.

Educational institutions should develop specialized programs to train engineers, technicians, and researchers in bladeless turbine technology. Collaboration between universities and industry can facilitate knowledge transfer and ensure the availability of a skilled workforce to support the deployment of this technology. Energy planners should explore the integration of bladeless turbines with renewable energy sources, such as wind, solar, and hydroelectric power. This integration can enhance overall system efficiency and provide a more stable and reliable energy supply. By implementing these recommendations, stakeholders can harness the full potential of bladeless turbine technology, leading to more efficient, sustainable, and resilient energy systems.

Further studies should focus on optimizing the geometrical design parameters of bladeless rotors, such as disc spacing, number of discs, and surface texture, to maximize efficiency and performance under various operating conditions. Also, conducting experiments with bladeless turbines of different scales, from small prototypes to full-scale models, will help validate the scalability of the technology and its performance in real-world applications.

REFERENCES

Sengupta, S., and Guha, A. (2018). Inflow-rotor interaction in Tesla disc turbines: Effects of discrete inflows, finite disc thickness, and radial clearance on the fluid dynamics and performance of the turbine. Procedure Institute. Mechanical. Engineering, Part A *Journal of Power and Energy*, **232:** 971–991.

Hamdan, H., Dol, S.S., Gomaa, A.H., Tahhan, A.B.A., Al Ramahi, A., Turkmani, H.F., Alkhedher, M., Ajaj, R. (2024). Experimental and Numerical Study of Novel Vortex Bladeless Wind Turbine with an Economic Feasibility Analysis and Investigation of Environmental Benefits. *Energies*, 17, 214. https://doi.org/10.3390/en17010214 .

Wang Q., Zhu, Z., Chen, W., and Zhou, Y. (2022). A new type of bladeless turbine for compressed gas energy storage system. Front Chem., ;10:1013473. doi: 10.3389/fchem.2022.1013473.

Onanuga, O.K., Erusiafe, N.E., Olopade, M.A., and Chendo, M.A.C. (2020), Experimental and analytical analysis of a bladeless turbine of an incompressible fluid in a confined cylinder. Elsevier Journal, Results in Engineering (6), 100130 doi.org/10.1016/j.rineng.2020.100130 , pages 1-10.

Olujobi, O. J., Okorie, U. E., Olarinde, E. S., Aina-Pelemo, A. D. (2023). Legal responses to energy security and sustainability in Nigeria's power sector amidst fossil fuel disruptions and low carbon energy transition. *Heliyon*. 9(7), e17912. doi: 10.1016/j.heliyon.2023.e17912.

Emetere, M. E., Agubo, O., and Chikwendu, L. (2021). Erratic electric power challenges in Africa and the way forward via the adoption of human biogas resources. *Energy Exploration & Exploitation*, **39**(4): 1349-1377.

Sani, Y., and Scholz, M. (2022). The interplay of Water–Energy Security and Food Consumption Patterns towards Achieving Nutrition Security in Katsina State, North- Western Nigeria, *Sustainability*, **14**(8): 4478.

Oyedepo, S.O. (2012). Energy and sustainable development in Nigeria: the way forward. *International Journal of energy and environmental engineering* **3** (1):178, 1-11.

Rice, W. (1965). "An Analytical and Experimental Investigation of Multiple-Disk Turbines", *Journal of Engineering for Power, Trans. ASME, series A*, **87** (1)**:** 29-36.

Cairns, W. J. (2003). *The Tesla disc turbine*, (Camden Miniature steam services, Great Britain). Second (revised) printing.

Song, J., Ren, X., Li, X., Gu, C., and Zhang,M. (2018). One- dimensional model analysis and performance assessment of Tesla turbine. *Applied Thermal Engineering, Science Direct journal*, **134**: 546-554.

Ciapp, L., Fiaschi,D., Niknam, P., and Talluri, L. (2019). Computational investigation of the flow inside a Tesla turbine rotor. *Energy*, **173**: 207 – 217.

Zhang, Y.; Cai, X.; Lin, S.; Wang, Y.; Guo, X. CFD Simulation of Co-Planar Multi-Rotor Wind Turbine Aerodynamic Performance Based on ALM Method. Energies 2022, 15, 6422. https://doi.org/10.3390/en15176422.

Rusin, K., Wróblewski, W., and Strozik, M. (2018). Experimental and numerical investigations of Tesla turbine. *Journal Phys. Conference Series*. **1101**: 012029.

Krzysztof, R., Włodzimierz, W.,and Michał, S. (2019). Comparison of methods for the determination of Tesla turbine performance. *Journal of Theoretical and Applied Mechanics* **57**(3): 563-575.

Tesla, N., (1913). *Turbine*. Patent no: 1,061,206. United States Patent Office, New York, Patented May 6, 1913.